Contrib Mineral Petrol (2013) 165:1225–1242
DOI 10.1007/s00410-013-0855-8

ORIGINAL PAPER

The origin of coarse garnet peridotites in cratonic lithosphere: new data on xenoliths from the Udachnaya kimberlite, central Siberia

Luc S. Doucet · Dmitri A. Ionov · Alexander V. Golovin

Received: 6 July 2012 / Accepted: 12 January 2013 / Published online: 12 February 2013

Abstract We report new textural and chemical data for 10 garnet peridotite xenoliths from the Udachnaya kimberlite and examine them together with recent data on another 21 xenoliths from the 80–220 km depth range. The samples are very fresh (LOI near zero), modally homogeneous and large (>100 g). Some coarse-grained peridotites show incipient stages of deformation with <10 % neoblasts at grain boundaries of coarse olivine. Such microstructures can only be recognized in very fresh rocks, because fine-grained interstitial olivine is strongly affected by alteration, and may have been overlooked in previous studies of altered peridotite xenoliths in the Siberian and other cratons. Some of the garnet peridotites are similar in composition to low-opx Udachnaya spinel harzburgites (previously interpreted as pristine melt extraction residues), but the majority show post-melting enrichments in Fe and Ti. The least metasomatized coarse peridotites were formed by 30–38 % of polybaric fractional melting between 7 and 4 GPa and ≤1–3 GPa. Our data together with experimental results suggest that garnet in these rocks, as well as in some other cratonic peridotites elsewhere, may be a residual mineral, which has survived partial melting together with olivine and opx. Many coarse and all deformed garnet peridotites from Udachnaya underwent modal metasomatism through interaction of the melting residues with Fe-, Al-, Si-, Ti-, REE-rich melts, which precipitated cpx, less commonly additional garnet. The xenoliths define a complex geotherm probably affected by thermal perturbations shortly before the intrusion of the host kimberlite magmas. The deformation in the lower lithosphere may be linked to metasomatism.

Keywords Garnet peridotite · Mantle xenolith · Craton · Melting residue · Metasomatism · Deformation

Communicated by T. L. Grove.

Electronic supplementary material The online version of this article (doi:10.1007/s00410-013-0855-8) contains supplementary material, which is available to authorized users.

L. S. Doucet (✉) · D. A. Ionov
Université J. Monnet (Member of PRES Université de Lyon),
42023 Saint Etienne, France
e-mail: luc.serge.doucet@univ-st-etienne.fr

L. S. Doucet · D. A. Ionov
UMR 6524 "Magmas et Volcans", CNRS,
42023 Saint Etienne, France

A. V. Golovin
V.S. Sobolev Institute of Geology and Mineralogy,
Siberian Branch, Russian Academy of Sciences,
Novosibirsk 630090, Russia

Introduction

Garnet peridotites are by far the most common rock type in cratonic mantle, particularly in the depth range 80–250 km (Boyd 1989; Lee et al. 2011; Pearson et al. 2003). Understanding their origin is essential to get a better insight into the origin of cratonic lithosphere. Garnet peridotites are usually considered to be residues of high degrees of melt extraction that experienced a range of post-melting chemical and modal enrichments commonly referred to as metasomatism and/or "re-fertilization" (Carlson et al. 2005; Ionov et al. 2010; Pearson et al. 1995; Shimizu et al. 1997; Simon et al. 2003), in many cases accompanied by deformation (Boyd and Mertzman 1987). This intrinsic complexity of the origin of garnet peridotites makes it difficult, on the one hand, to define their melting conditions (because of variable metasomatic imprints) and, on the

other hand, to trace a sequence of various enrichment events, which may have taken place in several stages. As a result, a large number of processes, tectonic settings and evolution paths have been proposed for the formation of garnet-facies cratonic mantle involving various residual peridotites and their interaction with intra-plate alkali-rich silicate or carbonatitic melts (Rudnick et al. 1993; Simon et al. 2003) or subduction-related melts/fluids (Kelemen et al. 1998; Pearson and Wittig 2008).

Tracing the melt extraction history of garnet-facies peridotites may be easier for xenolith suites that contain both garnet and spinel peridotites because the latter are usually less metasomatized and considered as being closer in modal and chemical composition to initial melting residues (Bernstein et al. 1998, 2007; Boyd 1989; Wittig et al. 2008). Some major insights into melting conditions and tectonic settings during the formation of cratonic mantle have been obtained through studies of spinel peridotites. A very promising approach to shed more light on the origin of garnet peridotites is to examine a large suite of cratonic peridotites including both garnet- and spinel-facies rocks suitable to obtain high-quality petro-geochemical data.

In this paper, we explore the origin of a unique suite of large, fresh and homogeneous garnet peridotite xenoliths from the Udachnaya kimberlite in the central Siberian craton (Agashev et al. 2013; Ashchepkov et al. 2010; Boyd et al. 1997; Ionov et al. 2010) in relation to a recent study that addressed the formation of spinel harzburgites from the same locality (Doucet et al. 2012). We report new modal, major and trace element data for 10 xenoliths and examine them together with recently published data on another 21 garnet peridotites (Ionov et al. 2010), which collectively represent an almost complete lithospheric mantle section beneath Udachnaya. We focus on the origin of "coarse" peridotites that experienced no or very little deformation. Our main objectives are to better constrain the formation conditions of initial "protoliths" of the garnet peridotites by partial melting (depths, melting degrees, tectonic settings) and the origin of garnet (residual vs. metasomatic), which have not been addressed in detail by earlier work on Udachnaya (Boyd et al. 1997; Ionov et al. 2010). We also examine the nature and sequence of processes that transformed the melting residues to the garnet-facies rocks sampled by kimberlite magmatism as well as links between their modal and chemical composition, microstructures and locations in the lithospheric profile.

Geological setting, sample selection and preparation

Xenoliths in this study are from the Udachnaya-East kimberlite (66°26′N, 112°19′E) erupted 360 Myr ago (Kinny et al. 1997) through the PR_2-AR_1 Daldyn block of the central Siberian craton (Rosen et al. 1994) (Fig. 1). Early studies of mantle materials at Udachnaya (Boyd et al. 1997; Spetsius and Serenko 1990; Zinchuk et al. 1993) were based on samples from shallow levels in the open-pit diamond mine, which are strongly serpentinized (LOI 3–15 % for peridotite xenoliths). Samples reported here were collected in 2003–2009 in the 420–640 m depth range near the centre of the pipe. They are hosted by remarkably well-preserved type-I kimberlites, which contain fresh, unserpentinized olivine and groundmass (Kamenetsky et al. 2008), and are basically unaffected by syn- and post-magmatic alteration (Kamenetsky et al. 2009a, b, 2012).

Large, homogeneous and fresh coarse-grained garnet peridotites, which contain unaltered olivine, garnet and pyroxenes (Fig. 2a), were selected among several hundred xenoliths. They are 15–30 cm in size and have ellipsoidal shapes. We rejected heterogeneous xenoliths, for example, those with cm-scale garnet-rich segregations (Fig. 2b), and rare rock types, like wehrlites, which may be of magmatic origin. The new samples are coarse or only moderately deformed; sheared peridotites examined in this study are from previous work (Table 1). A sufficiently large amount of fresh material (≥100 g taking into account grain size) was taken from xenolith cores to provide representative whole-rock samples (Boyd 1989) and was crushed to <5–10 mm in a steel jaw crusher. Splits of crushed samples (~50 g) were ground in agate to fine powder. Olivine, pyroxenes and garnet were handpicked from sieved 0.5–1.0 mm size fractions of the remaining material to produce grain mounts for micro-beam analyses.

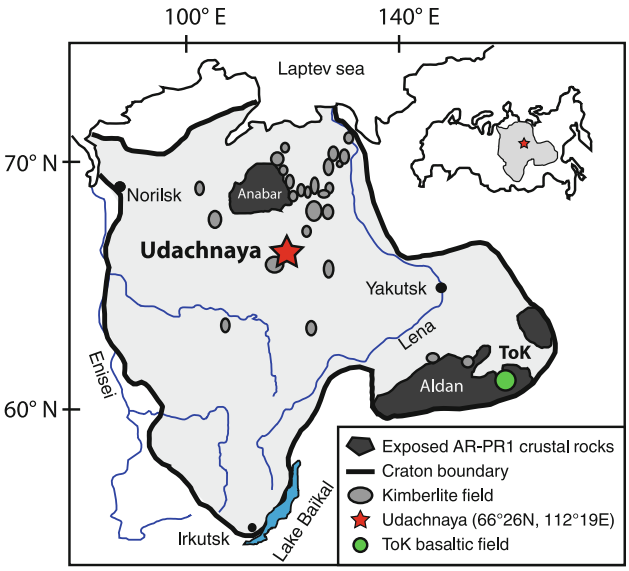

Fig. 1 Location map of Udachnaya, kimberlite fields and areas of exposed early Precambrian crust (Aldan and Anabar shield) in the Siberian craton. Adapted from Ashchepkov et al. (2010)

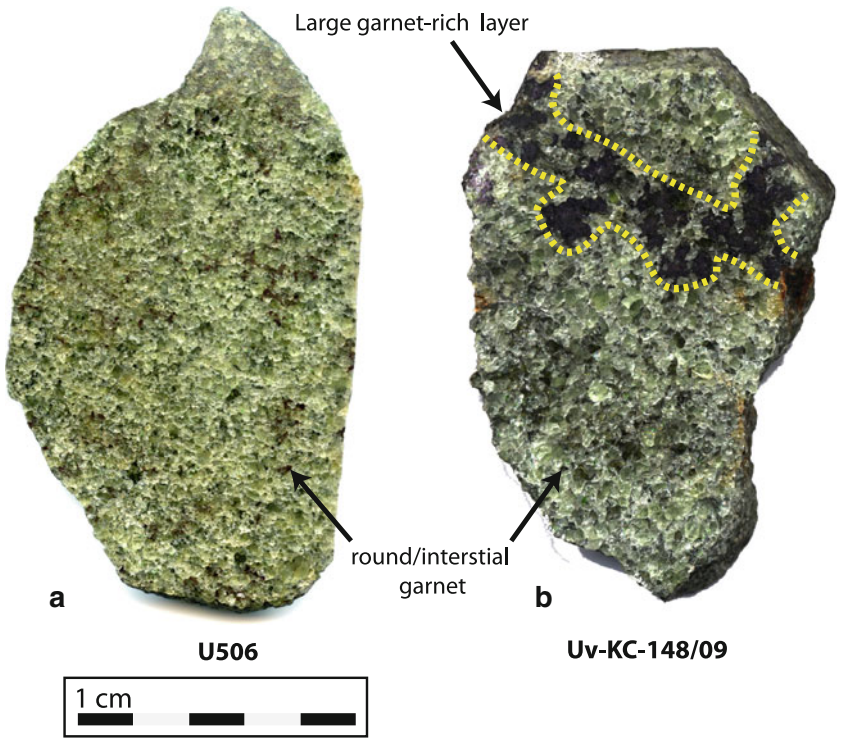

Fig. 2 Photographs of sawn hand specimens from fresh granular peridotite xenoliths collected at the Udachnaya kimberlite pipe. **a** Garnet harzburgite U506. **b** Heterogeneous garnet peridotite Uv-KC-148/09 collected together with peridotite xenoliths used in this study

Analytical methods

The abundances of major and minor elements in bulk-rocks were determined by wavelength-dispersive (WD) X-ray fluorescence (XRF) spectrometry at J. Gutenberg University, Mainz. The rock powders were first ignited for 3 h at 1,000 °C to convert all FeO into Fe_2O_3 and expel water and CO_2. Glass beads, produced by fusing 0.8 g of the ignited powders with 4.8 g of dried LiB_4O_7 (1:7 dilution), were analysed on a Philips PW1404 instrument using ultramafic and mafic reference samples as external standards. Reference sample JP-1 was run as an unknown to control precision and accuracy with results close to recommended values; full duplicates of Uv-KC-03/08 reproduced within 0.05 wt% for LOI, SiO_2, MgO and FeO, and $\leq$0.01 wt% for other elements (Online Resource 1).

Major element compositions of minerals were obtained by WD electron probe micro-analysis (EPMA) at Laboratoire Magmas et Volcans (LMV, Clermont-Ferrand) on a CAMECA SX-100 using 15 keV voltage, 15 nA sample current and counting times of 20–30 s for peaks and 10 s for background; standards were natural and synthetic minerals; ZAF correction was applied. The minerals were normally analysed in grain mounts, usually 4 different grains for clinopyroxene (cpx) and garnet, and 6 grains for olivine and orthopyroxene (opx), less commonly in thin sections to explore heterogeneities and zoning of mineral grains and their relation to textural position.

Whole-rock trace element compositions were determined by inductively coupled plasma mass-spectrometry (ICPMS) at Université Montpellier II following a modified method of Ionov et al. (1992). The powders (100 mg) were dissolved in HF-$HClO_4$. Dried samples were dissolved in HNO_3 and diluted in 2 % HNO_3 to 1:2,000 shortly before analysis. The solutions were analysed on an Element XR instrument together with four blanks, three duplicates (separate dissolutions) and two duplicates of JP-1. Chemical blanks were 0.5 ppm for Ba, 0.002–0.1 ppm for Li, Sr, Zr and Rb, 0.01–0.001 ppm for Y, Nb, La, Ce, Hf and Th, and <0.001 ppm for other rare earth elements (REE), Ta and U.

Minerals were analysed for trace elements by laser-ablation (LA) ICPMS in grain mounts at the LMV. The AGILENT 7500 ICPMS instrument is coupled with an Excimer 193 nm Resonetics M-50E ATL operated at 7 Hz, 6 mJ cm^{-2} pulse energy and 70–100 μm beam size. Helium was used as carrier gas. Acquisition time was 90 s for background and 60 s for each signal. Reference sample SRN NIST 612 was used as an external standard (Gagnon et al. 2008). Data were reduced with GLITTER software.

Petrography

Photomicrographs of representative xenoliths are shown in Fig. 3; those for all xenoliths in this study (full-size images

Table 1 Summary of petrological data for Udachnaya xenoliths in this study

Sample no	WR (g)	Rock type	Mg# (ol)	Cr# (gar)	*P* (GPa)	*T*, °C (Ca-opx)	*P* (GPa)	*T*, °C (Taylor)	Calculated modal abundances, wt%			
									ol	opx	cpx	gar
Coarse garnet peridotites												
Uv-02/03	90	Hzb	0.925	0.243	4.5	848	–	–	80.2	15.9	0.0	3.9
Uv-604/09	188	Hzb	0.924	0.150	3.5	939	–	–	84.6	10.7	0.0	4.7
Uv-419/09	380	Hzb	0.922	0.164	5.0	931	5.1	952	69.4	21.5	4.5	4.6
U29	390	Lh	0.922	0.183	5.3	940	5.1	886	68.6	20.2	5.6	2.1
U64	150	Hzb	0.909	0.336	6.0	1,175	6.2	1,219	77.1	16.6	3.8	2.5
U260	350	Hzb	0.917	0.223	3.5	846	–	–	90.0	4.5	4.5	1.0
U280	510	Hzb	0.919	0.127	3.6	909	2.7	720	85.1	9.3	1.3	4.3
U283	143	Hzb	0.920	0.149	3.6	883	3.2	796	84.5	10.2	1.4	3.7
U501	220	Hzb	0.917	0.149	4.8	873	4.9	882	82.4	6.6	4.3	6.7
U506	190	Hzb	0.925	0.187	6.1	1,031	5.5	943	77.2	16.0	2.6	4.2
U508	110	Hzb	0.923	0.159	3.3	844			85.4	7.9	0.0	6.7
U1147	140	Hzb	0.925	0.139	5.1	991	4.7	915	64.5	26.4	1.0	8.1
U1188	200	Hzb	0.916	0.270	6.6	1,318	6.6	1,322	69.9	23.1	2.0	5.0
Transitional garnet peridotites												
Uv-01/03	160	Hzb	0.917	0.365	6.2	1,251	–	–	62.6	33.0	0.0	4.4
Uv-408/09	350	Hzb	0.908	0.170	6.3	1,300	6.4	1,301	67.4	22.0	4.2	6.4
Uv-103/03	133	Hzb	0.914	0.413	6.5	1,300	6.5	1,305	81.1	13.8	3.5	1.6
Uv-421/09	510	Hzb	0.908	0.210	5.6	1,256	5.7	1,278	70.9	20.8	3.5	4.8
Uv-573/09	270	Lh	0.911	0.144	6.0	1,283	6.1	1,289	69.6	17.4	5.6	7.4
Uv-KC-03/08	277	Hzb	0.910	0.181	6.3	1,294	6.3	1,305	83.2	9.4	4.1	3.3
Uv-KC-67/08	280	Hzb	0.912	0.243	6.2	1,286	6.3	1,300	68.7	23.3	3.9	4.1
U4	204	Lh	0.912	0.214	5.8	1,283	5.8	1,301	70.8	19.3	5.5	4.4
U10	200	Hzb	0.911	0.302	6.2	1,273	6.3	1,298	81.4	12.1	4.0	2.5
U50	220	Lh	0.910	0.140	6.1	1,297	6.1	1,294	65.2	22.0	5.9	6.9
U71	310	Lh	0.912	0.176	6.4	1,306	6.3	1,296	76.5	11.2	4.7	7.6
Sheared garnet peridotites												
U9	220	Hzb	0.905	0.294	5.8	1,252	–	–	70.3	24.1	0.0	5.6
U57	550	Hzb	0.911	0.341	6.5	1,291	6.5	1,299	85.2	8.5	4.0	2.3
U70	410	Lh	0.901	0.154	5.2	1,224	5.2	1,235	79.0	9.5	6.0	5.5
U148	91	Lh	0.906	0.139	5.9	1,258	6.0	1,271	69.7	16.4	6.2	7.7
U183	190	Hzb	0.915	0.285	6.3	1,198	6.5	1,244	80.8	13.5	1.9	3.8
U503	140	Hzb	0.912	0.313	6.4	1,283	6.6	1,320	75.2	14.0	3.7	7.1
U532	204	Lh	0.910	0.311	5.8	1,277	5.8	1,289	86.4	5.7	4.9	3.0

Samples with prefix "Uv" are from this study, those with prefix "U" are from Ionov et al. (2010). Hzb, harzburgite; Lh, lherzolite. Transitional peridotites contain <10–20 % of anhedral neoblasts; the neoblasts in sheared peridotites are smaller and may make up 60–90 % of total olivine. WR, weight of crushed whole-rock samples. Mg#, $Mg/(Mg + Fe)_{at}$; Cr#, $Cr/(Al + Cr)_{at}$. Ol, olivine; opx, orthopyroxene; cpx, clinopyroxene; gar, garnet. Equilibration pressures (*P*) and temperatures (*T*) are from Nickel and Green (1985) opx-gar barometer, Taylor (1998) cpx-opx thermometer and Brey and Köhler (1990) Ca-in-opx thermometer corrected as in Nimis and Grütter (2010). Modal estimates were obtained by least-squares from whole-rock and mineral major oxide compositions

of 4.5 cm × 2.5 cm sections in transmitted plane-polarized and cross-polarized light) are given in Online Resource 2. Based on microstructures, they are grouped into coarse, transitional and sheared.

Only three out of ten new medium- to coarse-grained xenoliths selected for this study can be considered as classical "coarse" peridotites with protogranular to mosaic equigranular microstructures (Fig. 3a, b). Another seven contain small amounts (usually <10 %) of anhedral olivine neoblasts and sub-grains at rims of coarse, strained olivine (Fig. 3c, d) and thus must be, strictly speaking, classified as porphyroclastic even though the contents of neoblasts are very low. Following Ionov et al. (2010), we classify such xenoliths as "transitional" (between coarse and sheared),

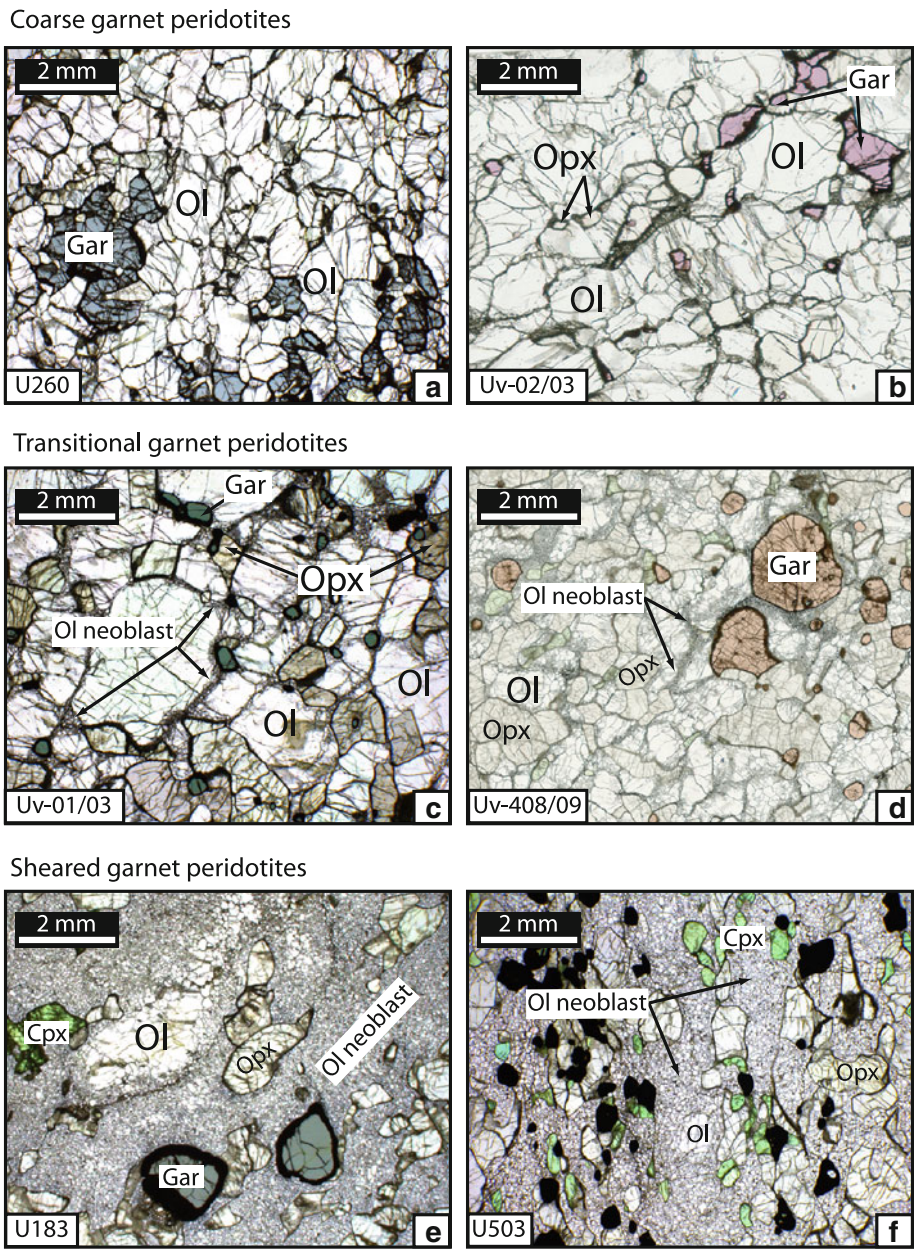

Fig. 3 Photomicrographs of garnet peridotites from Udachnaya in transmitted plane-polarized light showing representative microstructures; scale bars are at *upper left*, sample numbers are at *bottom left*. *Ol* Olivine, *Opx* orthopyroxene, *Cpx* clinopyroxene, *Gar* garnet. Two samples are shown for each microstructural type: **a–b** coarse, **c–d** transitional (incipient deformation, rare subgrains and neoblasts at rims of coarse olivine), **e–f** sheared (olivine mainly as fine-grained neoblasts)

that is, showing incipient stages of deformation. The transitional microstructures with rare neoblasts essentially restricted to grain boundaries of coarse olivine (Fig. 3c, d) can only be recognized in very fresh rocks, like those in this work because fine-grained interstitial olivine is the first to be affected by alteration. We argue that such microstructures may have been overlooked in previous studies of altered peridotite xenoliths in the Siberian and other cratons. If this is correct, some data on "coarse" cratonic peridotites in the literature may actually have been obtained on transitional rocks with low deformation degrees.

Together with xenoliths initially reported by Ionov et al. (2010), 13 samples in this study are coarse and 11 transitional. Nearly all (19 out of 24) are harzburgites (≤5 % cpx; four are cpx-free), five are low-cpx lherzolites (5–6 % cpx). Olivine usually has equant shapes and larger grains than opx (Fig. 3a–d); cpx forms small grains in the vicinity of opx. Garnet (1–8 %) ranges from rare interstitial grains to large irregular aggregates or equant grains with smooth boundaries (Fig. 3a). Seven sheared peridotites are harzburgites or low-cpx lherzolites (5–6 % cpx) and contain 2–7 % garnet. They are porphyroclastic, usually with >50 % of olivine as fine-grained neoblasts (Fig. 3e, f) and

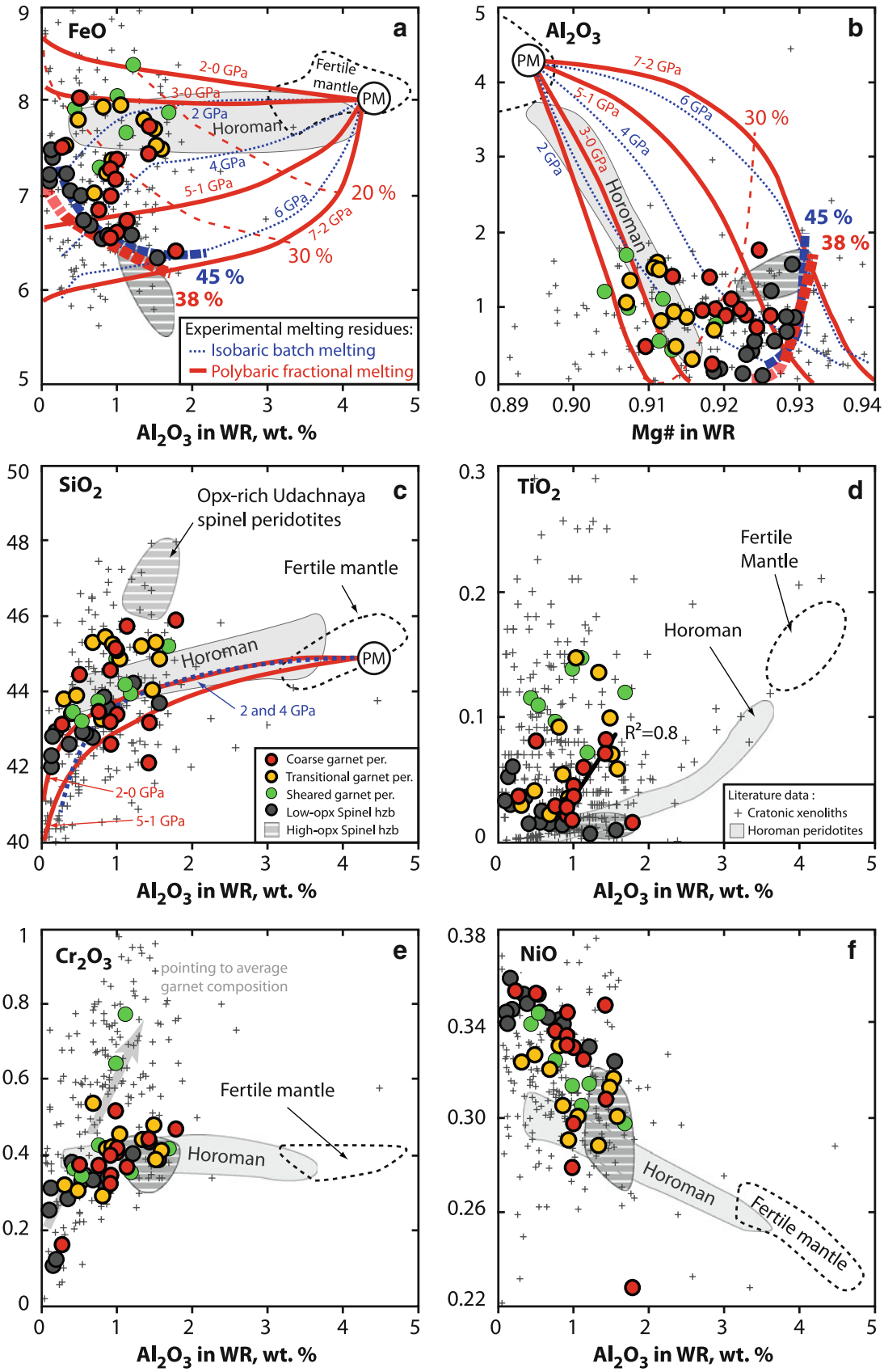
FeO
a
2-0 GPa
3-0 GPa
2 GPa
Horoman
4 GPa
5-1 GPa
6 GPa
7-2 GPa
Fertile mantle
PM
20 %
30 %
45 %
38 %
Experimental melting residues:
Isobaric batch melting
Polybaric fractional melting
Al2O3 in WR, wt. %
Al2O3
b
PM
7-2 GPa
6 GPa
5-1 GPa
4 GPa
3-0 GPa
2 GPa
Horoman
30 %
45 %
38 %
Mg# in WR
SiO2
c
Opx-rich Udachnaya
spinel peridotites
Fertile mantle
Horoman
PM
2 and 4 GPa
2-0 GPa
5-1 GPa
Coarse garnet per.
Transitional garnet per.
Sheared garnet per.
Low-opx Spinel hzb
High-opx Spinel hzb
Al2O3 in WR, wt. %
TiO2
d
Fertile
Mantle
Horoman
R²=0.8
Literature data :
Cratonic xenoliths
Horoman peridotites
Al2O3 in WR, wt. %
Cr2O3
e
pointing to average
garnet composition
Fertile mantle
Horoman
Al2O3 in WR, wt. %
NiO
f
Horoman
Fertile mantle
Al2O3 in WR, wt. %

◀ **Fig. 4** Co-variation plots of major and minor oxides (wt%) and Mg# [$Mg/(Mg + Fe)_{at}$] for coarse, transitional and sheared whole-rock garnet peridotites from Udachnaya in this study [see (**a**), (**c**) and (**d**) for symbols]. Also shown are primitive mantle (PM) after McDonough and Sun (1995); fertile off-craton garnet and spinel peridotite xenoliths from Vitim and Tariat in central Asia (*fine black dashed lines*; Ionov et al. 2005a; Ionov and Hofmann 2007); low-opx (*dark grey circles*) and high-opx (*grey dashed field*) spinel peridotites from Udachnaya after Doucet et al. (2012); Horoman massif peridotites (*grey* contours; Takazawa et al. 2000); cratonic peridotite xenoliths (*thin crosses*) from the Kaapvaal (Simon et al. 2007; Pearson et al. 2004), Tanzanian (Lee and Rudnick 1999), North Atlantic (Bernstein et al. 1998, 2006; Wittig et al. 2008) and Slave (Irvine et al. 2003; Kopylova and Russell 2000) cratons. *Thin dashed blue lines* show isobaric batch melting residues formed at 2, 4 and 6 GPa; continuous red lines are residues of polybaric fractional melting at 2–0, 3–0, 5–1 and 7–2 GPa (Herzberg 2004). *Thick dashed blue lines* show residues of 45 % batch melting between 2 and 6 GPa; thick dashed red lines show 38 % of polybaric fractional melting

relics of strained olivines with abundant sub-grains. Proportions of coarse and neoblastic olivine, as well as the size of the neoblasts, may vary locally. Pyroxenes are elongated and commonly show alteration at rims and cracks (Fig. 3e). Garnets are often round; they range in size from tiny grains to >2 mm and usually have thick kelyphitic rims (Fig. 3e, f). The recrystallization shows little, if any, effect on garnet.

Even though we took care to avoid xenoliths with kimberlite veins, some interstitial kimberlite-related materials, sometimes with late-stage phlogopite, were found in thin sections in some samples (Online Resource 3). They may affect whole-rock abundances of alkalis, but not of major oxides (Si, Mg, Al, Fe), whose contents in the kimberlites are not very different from those in the peridotites (Kamenetsky et al. 2012).

Major element and modal compositions

Whole-rock (WR) major oxide and LOI data are given in Online Resource 1 and are shown as co-variation plots in Fig. 4. The LOI values range from 1.5 % to −0.5 % (average 0.3 %); they indicate that secondary alteration is limited, that is, nearly absent in many samples and low in others, even in samples with fine-grained olivine sensitive to alteration. The negative LOI, that is, gain of mass on ignition (up to 0.5 %) means that oxidation of FeO to Fe_2O_3 is more significant than the loss of volatiles (usually H_2O and CO_2 from alteration products) if the latter are present.

Coarse and deformed peridotites have similar ranges of SiO_2 (42–46 %), Al_2O_3 (0.3–1.8 %) and CaO (0.6–1.7 %), but coarse peridotites tend to have higher $Mg\#_{WR}$ [$Mg/(Mg + Fe)_{at}$] (average: ~0.920 vs. 0.912) and lower FeO (average: 7.1 vs. 7.7 %); sheared peridotites have the highest TiO_2 (Fig. 4).

On diagrams of Al_2O_3 versus FeO and Mg# (Fig. 4a, b), some coarse garnet peridotites plot close to low-opx spinel peridotites from Udachnaya, which were previously interpreted as pristine melting residues based on Al–Fe–Mg# relations in comparison with experimental data (Doucet et al. 2012). The majority of coarse garnet peridotites, however, have higher FeO at given Al_2O_3 than the spinel peridotites, that is, show Fe-enrichments relative to inferred melting residues. The garnet peridotites also tend to have higher TiO_2 than the spinel peridotites and residual peridotite suites, for example, the Horoman massif (Fig. 4d). Some garnet peridotites have slightly higher SiO_2 than the low-opx spinel peridotites (average: 44.5 vs. 43 %) (Fig. 4c), but none contains as much silica as opx-rich spinel peridotites from Udachnaya (average 46.8 %). The range of Cr_2O_3 in garnet peridotites (0.12–0.78 %) extends to higher values than in the spinel peridotites (0.1–0.4 %), but very high Cr_2O_3 (>0.6 %), common in published data on cratonic peridotites, was found only in two sheared, garnet-rich samples in our suite (Fig. 4e). The contents of NiO in many coarse peridotites are close to those in spinel peridotites (0.33–0.35 %), but the deformed rocks (and four coarse peridotites with >20 % opx) have lower NiO (0.23–0.33 %; Fig. 4f).

EPMA obtained in this study is given in Online Resource 1. Mineral grains are normally not zoned. Mg# of olivine ($Mg\#_{Ol}$) ranges from 0.900 to 0.925 and is generally lower in deformed (0.900–0.917) than in coarse garnet peridotites, the latter commonly have $Mg\#_{Ol} \geq 0.92$, which overlap the lowest $Mg\#_{Ol}$ in spinel peridotites (Fig. 5a–c). $Mg\#_{Ol}$ and $Mg\#_{Opx}$ define a positive linear co-variation (Fig. 5a), indicative of equilibrium Mg–Fe distribution between olivine and opx. By contrast, $Mg\#_{Ol}$ shows no regular correlation with Mg# in coexisting cpx (Fig. 5a). This may either indicate that cpx in many garnet peridotites is not chemically equilibrated with coexisting olivine and thus may be of late-stage origin or be due to the effects of pressure and temperature on cpx-garnet equilibria (Brey and Köhler 1990). The contents of Al_2O_3 in opx from garnet peridotites are lower than in opx from nearly all spinel peridotites (except four ultra-depleted rocks with <0.2 wt% Al_2O_3) because Al strongly partitions to garnet; Al_2O_3 in opx is negatively correlated with $Mg\#_{Ol}$ in deformed peridotites (Fig. 5b).

Classification schemes for mantle-derived garnets are mainly based on their Ca–Cr relations (Grütter et al. 2004; Sobolev 1974). CaO and Cr_2O_3 contents of garnets in this study range broadly and are positively correlated (Fig. 5d) as is common for garnets in cratonic peridotite xenoliths (Grütter et al. 2004; Pearson et al. 2003). Only one garnet (from coarse cpx-free sample Uv-02/03) can be classified as "harzburgitic" G10 (low-Ca), the most abundant type recovered in diamond exploration the world over, which is

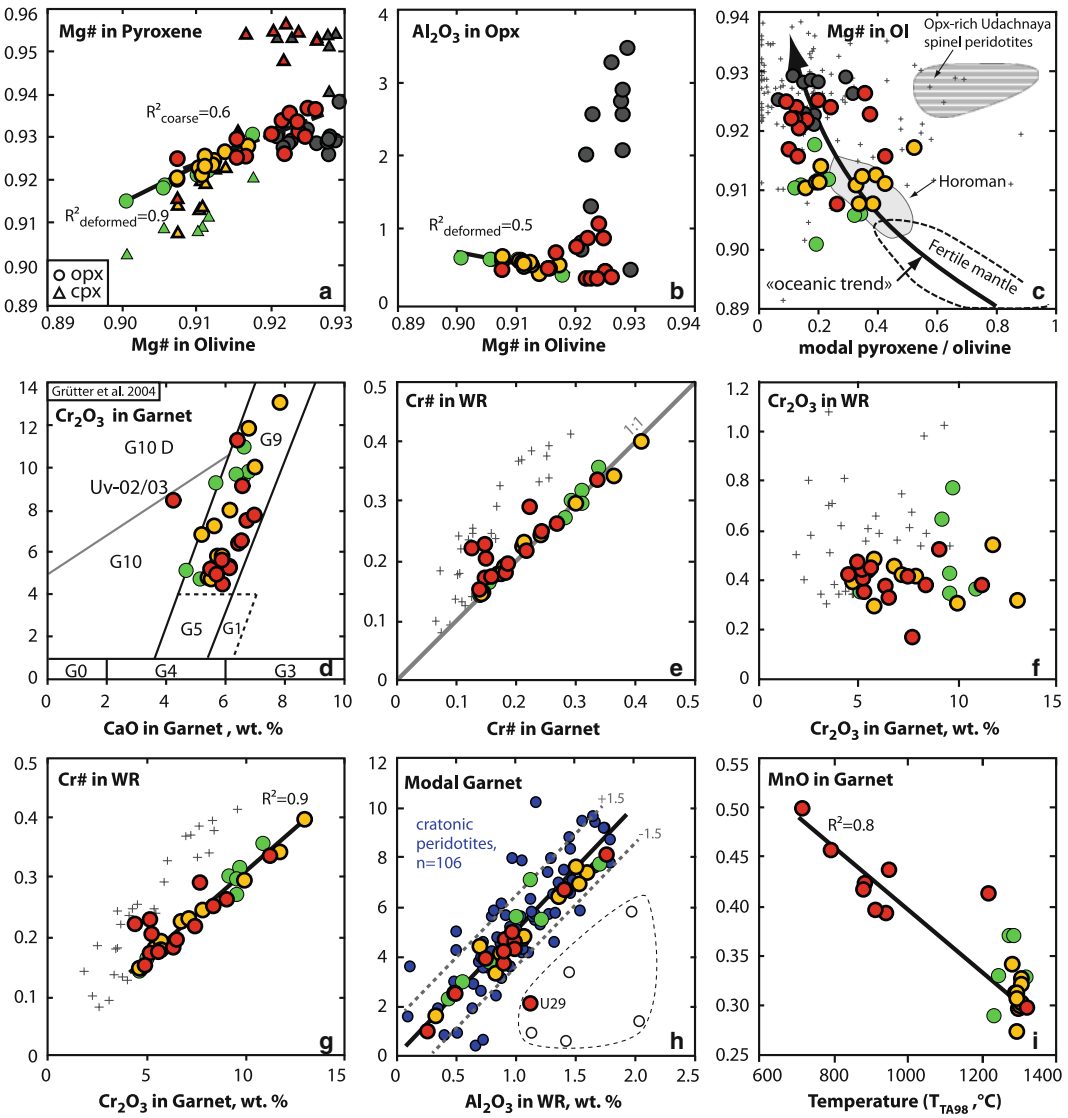

Fig. 5 Co-variation plots of major element and modal abundances (wt%) and ratios for olivine, pyroxenes and garnet from Udachnaya peridotites. **a** $Mg\#_{Ol}$ [$Mg/(Mg + Fe)_{at}$ in olivine] versus $Mg\#_{opx}$ and $Mg\#_{cpx}$; **b** $Mg\#_{Ol}$ versus Al_2O_3 in opx; **c** modal pyroxene/olivine versus $Mg\#_{Ol}$; **d** classification scheme for mantle-derived garnet from Grütter et al. (2004); **e** Cr# [$Cr/(Cr + Al)_{at}$] in garnet versus Cr# in WR; **f** Cr_2O_3 in garnets versus Cr_2O_3 in WR and **g** Cr# in WR; **h** Al_2O_3 in WR versus modal garnet for Udachnaya garnet peridotites (this study) and for worldwide cratonic peridotites (*blue circles* Boyd et al. 1997; Lee and Rudnick 1999; Kopylova and Russell 2000; Irvine et al. 2003; Simon et al. 2007; Pearson et al. 2004; Wittig et al. 2008; fine *dashed lines*, cpx- and spl-rich peridotites); **i** Equilibration temperature after Taylor (1998) (T_{TA98}) versus MnO in garnet. Also shown are Horoman peridotites, fertile off-craton mantle and worldwide cratonic peridotite xenoliths [see Fig. 4 for symbols and references]

believed to originate from cpx-free rocks (Grütter et al. 2004). Garnets from all other samples in this study, including four cpx-free harzburgites, fall into the "lherzolitic" G9 field (Fig. 5d). $Cr\#_{Gar}$ [$Cr/(Cr + Al)_{at}$ in garnet] are identical to $Cr\#_{WR}$ in the deformed, and all but four, coarse peridotites, the latter showing slightly higher $Cr\#_{WR}$ like many samples from literature (Fig. 5e). $Cr\#_{Gar}$ show a positive correlation with CaO and a negative correlation with MgO. The contents of Cr_2O_3 in garnets are not correlated with whole-rock Cr_2O_3 (Fig. 5f), but show an excellent ($r^2 = 0.9$) positive linear correlation with $Cr\#_{WR}$ (Fig. 5g). Cr# appears to be a very useful chemical parameter of mantle garnets because it offers direct links to whole-rock chemistry.

Modal abundances were calculated from major element compositions of bulk-rocks and minerals. On average, coarse peridotites have slightly higher modal olivine (78 vs. 75 %), lower opx (14.5 vs. 16.4 %) and cpx (2.4 vs. 4 %) than deformed peridotites, but similar garnet (~5 %; Fig. 6a). Coarse garnet peridotites plot close to spinel peridotites on a diagram of $Mg\#_{Ol}$ versus pyroxene/olivine ratios, but generally apart from deformed peridotites

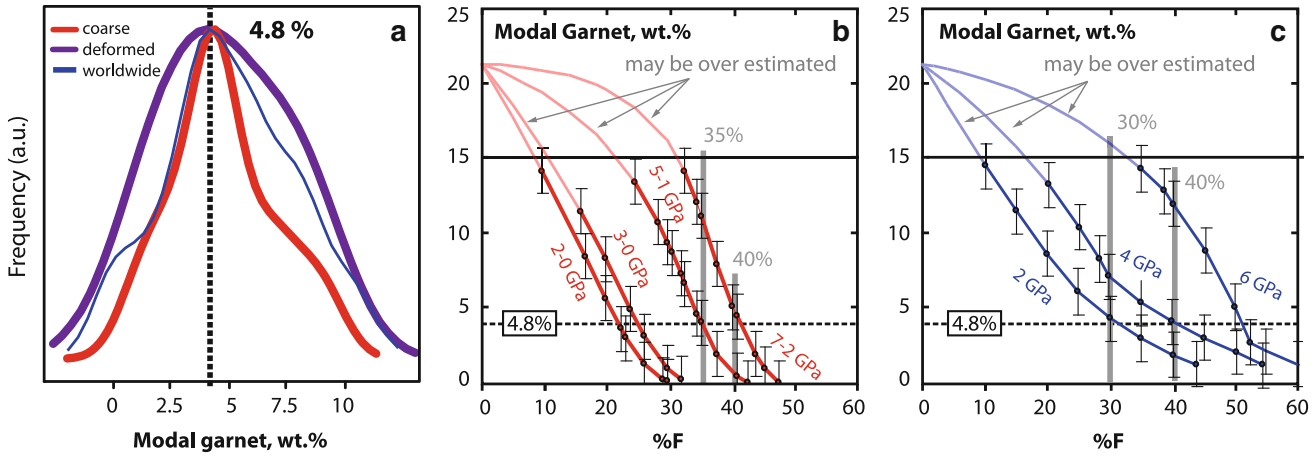

Fig. 6 **a** Frequency distribution diagram for modal garnet in coarse (*red line*) and deformed (*purple line*) peridotite xenoliths from Udachnaya and worldwide cratonic peridotite xenoliths (*blue line*) [see Fig. 5 for references]. **b–c** Calculated modal garnet in melt residues versus degree of partial melting (%F) for polybaric fractional melting (**b**) and isobaric batch melting (**c**). Modal garnet in melting residues in experiments of Herzberg (2004) was estimated as follows: Garnet (%) = Al_2O_3 (wt% in WR) × 5−0.15 defined by a linear correlation between Al_2O_3 in WR and modal garnet for cratonic peridotites (Fig. 5h). The equation is well constrained (error 1.5 %) for Al_2O_3 ≤2 % (12 % garnet), that is, modal garnet may be overestimated for Al_2O_3 >2 %. *Horizontal dashed lines* in **b–c** show the most common modal garnet values (4.8 %) in peridotites from Udachnaya and worldwide cratons; *thick grey vertical lines* show melting degree estimates for different pressures at 4.8 % residual garnet

(Fig. 5c), which is similar to cratonic peridotites elsewhere (Pearson and Wittig 2008; Simon et al. 2007). Modal garnet is positively correlated with whole-rock Al_2O_3 ($r^2 = 0.9$) (Fig. 5h). A comparison with literature data shows that such linear correlation may be a general feature of cratonic garnet peridotites. Thus, garnet abundances are controlled by whole-rock Al_2O_3 while garnet major oxide composition mainly depends on $Cr\#_{WR}$ or Cr/Al_{WR}.

Temperature and pressure estimates

Equilibration pressures (P) and temperatures (T) were calculated from average core compositions of minerals using several poly- and mono-mineral thermobarometers commonly applied to cratonic peridotites: the cpx-opx thermometer of Taylor (1998) (T_{TA98}), the Ca-in-opx thermometer of Brey and Köhler (1990) ($T_{Ca\text{-}in\text{-}opx}$) corrected by Nimis and Grütter (2010), the opx-gar barometer of Nickel and Green (1985) (P_{NG85}) as well as the single-cpx thermo-barometer of Nimis and Taylor (2000) (P_{NT00}–T_{NT00}) and the single-garnet thermo-barometer of Ryan et al. (1996) (P_{Cr}–T_{Ni}). The latter is based on the abundances of Cr (for P) and Ni (for T) and is mainly used to outline cratonic geotherms from data on garnet xenocrysts if no garnet peridotite xenoliths are available (Griffin et al. 1999). A recent re-assessment of thermo-barometry methods (Nimis and Grütter 2010) considers the P_{NG85}–T_{TA98} combination the most accurate for mantle peridotites.

The P_{NG85}–T_{TA98} estimates (Table 1; Fig. 7a) define a broad P–T range for coarse peridotites (2.7–6.6 GPa, 720–1,322 °C) and a narrow P–T range for deformed peridotites (5.2–6.6 GPa, 1,235–1,320 °C). They suggest a lithosphere-asthenosphere boundary beneath Udachnaya at ~7 GPa (~220 km) and show that both deformed and coarse peridotites occurred near the base of the lithosphere at the time of kimberlite eruption (~360 Ma). P–T values from most other methods yield somewhat different ranges (Table 1; Fig. 7b, c) but are generally consistent with the P_{NG85}–T_{TA98} estimates, that is, are scattered between the 35 and 45 mW m^{-2} model conductive geotherms (Pollack and Chapman 1977) and define no single P–T gradient, similar to published data for Udachnaya xenoliths obtained using different samples and methods (Boyd et al. 1997; Goncharov et al. 2012; Ionov et al. 2010).

The single-garnet thermo-barometer of Ryan et al. (1996) yields coherent P–T estimates for low-T (≤1,050 °C) peridotites, which plot between the 35 and 40 mW m^{-2} conductive geotherms, but unrealistic values (low P, high T) for high-T peridotites, which plot above the graphite/diamond boundary and partly on the mantle adiabate (Fig. 7d). This method, calibrated assuming Cr equilibrium between garnet and Cr-rich spinel, underestimates pressure if spinel is absent. The agreement between the single-garnet and poly-mineral thermo-barometers for the low-T Udachnaya peridotites may imply that their garnets are in equilibrium with Cr-spinel, that is, that accessory spinel may be present in some of the rocks, or that garnet peridotites are intercalated with spinel peridotites on a metre scale. The latter is consistent with overlapping T estimates for the Udachnaya spinel and low-T garnet peridotites (Doucet et al. 2012; Goncharov et al.

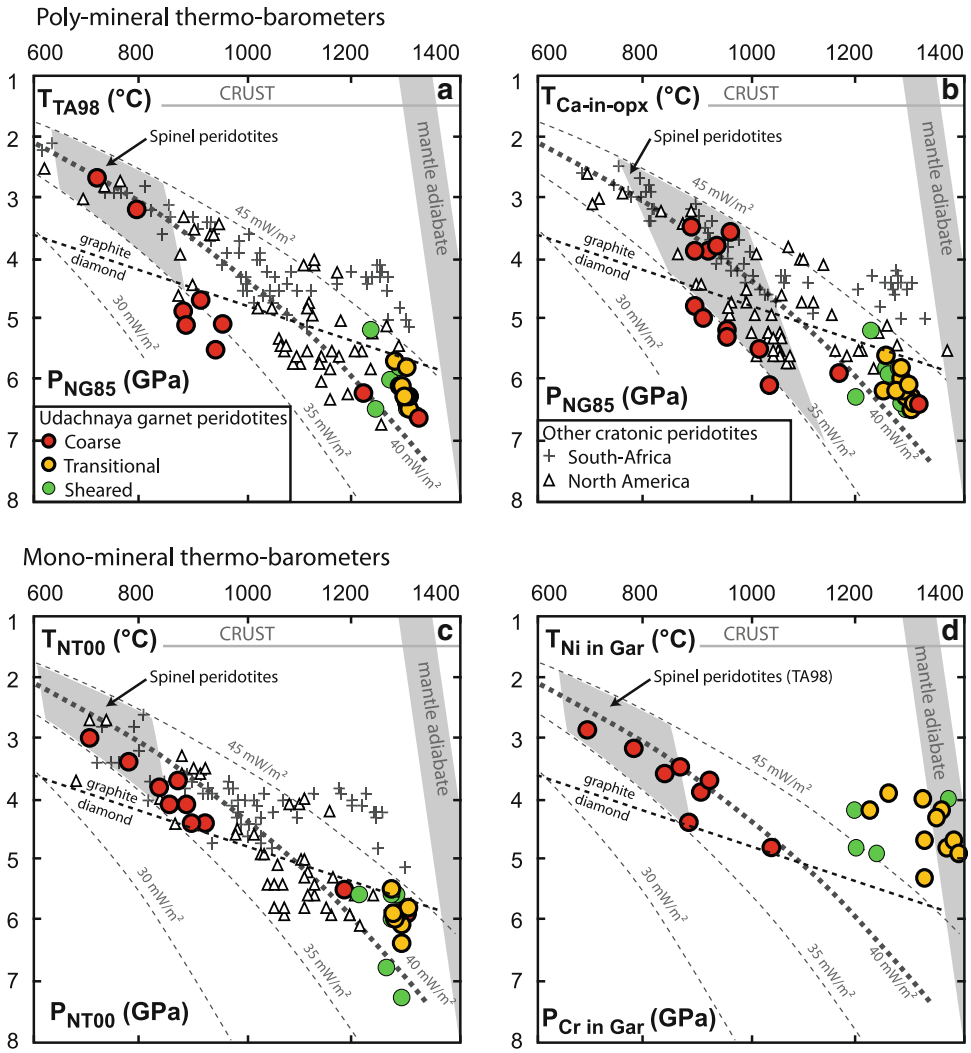

Fig. 7 Plots of equilibration temperature (T) versus pressure (P) for Udachnaya peridotites in this study. **a** P_{NG85}–T_{TA98}, **b** P_{NG85}–$T_{Ca\text{-}in\text{-}opx}$, **c** P_{NT00}–T_{NT00} and **d** P_{Cr}–T_{Ni} [see Fig. 4 for symbols and text for references and details]. P–T fields (*grey*) for spinel peridotites were calculated based on T estimates assuming that the samples plot between the 35 and 45 mW m^{-2} conductive geotherms of Pollack and Chapman (1977) (*grey dashed lines*). Also shown are mantle adiabate and the graphite-diamond transition boundary (Rudnick and Nyblade 1999) as well as P–T estimates for garnet peridotite xenoliths from South Africa (small *black crosses* Simon et al. 2007; Boyd et al. 2004) and North America (*triangles* Kopylova and Caro 2004; Sand et al. 2009; Wittig et al. 2008; Schmidberger and Francis 1999) re-calculated with the same thermo-barometers as for samples in this study

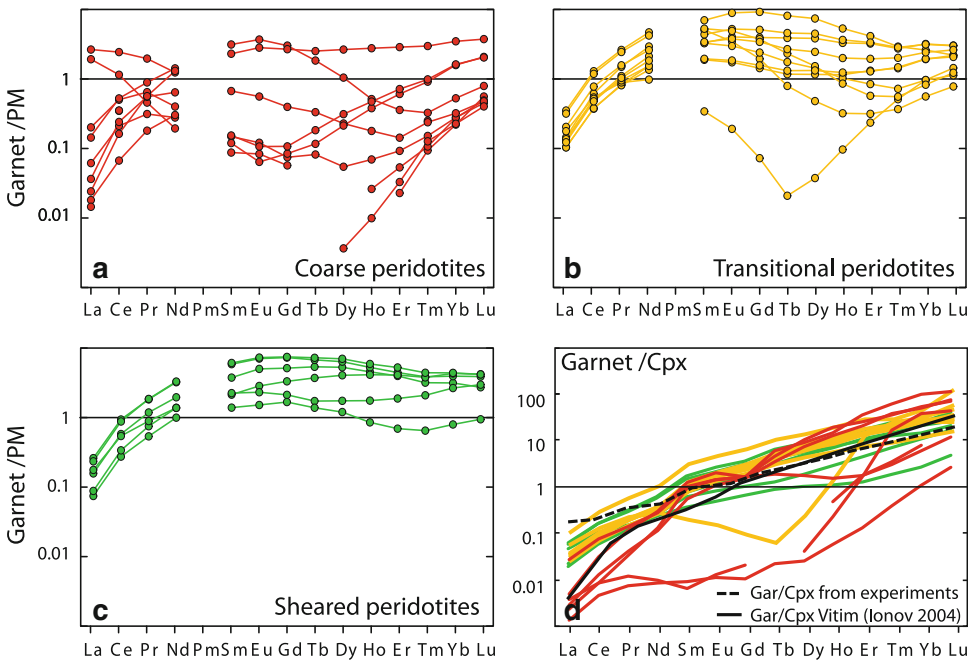

Fig. 8 Primitive mantle-normalized (McDonough and Sun 1995) rare earth element (REE) patterns for garnet in coarse (**a**), transitional (**b**) and sheared (**c**) Udachnaya peridotites, and **d** REE partitioning between garnet and cpx ($D^{gar/cpx}$) for Udachnaya peridotites in this study, off-craton peridotite xenoliths from Vitim (*black line* (Ionov 2004) and experimental data compiled for pMELTS software (*dashed black line* (Ghiorso et al. 2002; Smith and Asimow 2005)

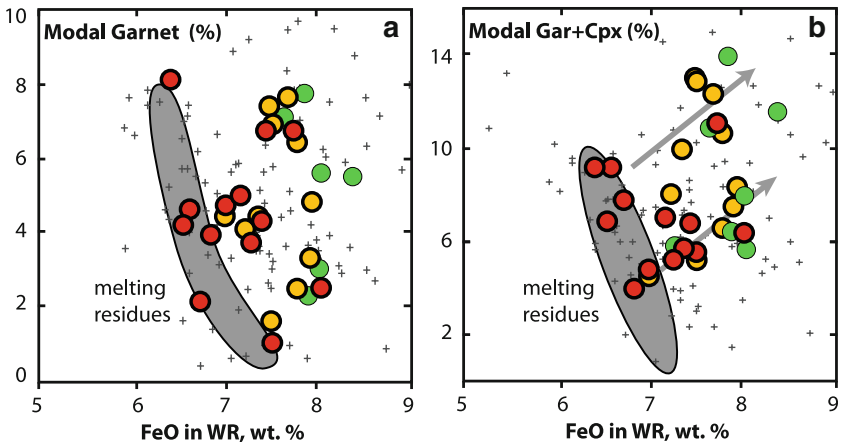

Fig. 9 Co-variation plots of FeO (wt%) in WR garnet peridotites from this study versus modal garnet (**a**) and modal garnet + cpx (**b**) in comparison with the field (*grey*) for melting residues estimated from Udachnaya spinel peridotites (Doucet et al. 2012) and worldwide cratonic garnet peridotites (*crosses*, see Fig. 4 for references)

2012; Ionov et al. 2010). To sum up, the method of Ryan et al. (1996) applied to our samples may only be valid at ≤4–5 GPa (130–150 km) and ignores the complexity of the perturbed local geotherm. The application of this technique to assess variations of mantle compositions with depth for the Siberian craton (Griffin et al. 1999), in particular at >130 km, does not appear to yield valid results and is not consistent with the vertical distribution of rock types established by xenolith studies (Ionov et al. 2010).

The contents of MnO in garnets from this study are negatively correlated with equilibration *T* (Fig. 5i) and show no correlation with other oxides in garnet or with MnO in olivine. Mn-in-garnet thermometers for cratonic mantle were earlier proposed by Delaney et al. (1979) and Creighton (2009). The broad *T* range for coarse Udachnaya peridotites also affects the *T*-dependant Fe–Mg distribution between olivine and opx (Mori and Green 1978), which shows more scatter for coarse than for deformed peridotites relative to $Mg\#_{Ol}$ versus $Mg\#_{Opx}$ co-variation trends (Fig. 5a) and explains the lack of correlation of Mg# with major oxides in garnet.

Trace element compositions

LA-ICPMS analyses of garnet, cpx and opx are given in Online Resource 1 and are shown as trace element patterns normalized to primitive mantle (PM; McDonough and Sun (1995) in Fig. 8 and Online Resource 4. Garnets show a broad range of REE patterns, from LREE-MREE-depleted to "sinusoidal" and "humped" (high-MREE). In the majority of coarse peridotites, garnets show depleted to sinusoidal REE, except U501, which has nearly flat MREE-HREE with LREE-depletion. Garnets in transitional and sheared rocks tend to have higher MREE with mildly sinusoidal to humped patterns (Fig. 8a–c). Clinopyroxenes generally show continuous enrichments from HREE to MREE and LREE, sometimes with nearly flat LREE, and only minor differences between coarse and deformed peridotites. Gar/cpx ratios for REE ($D^{gar/cpx}$) in several coarse peridotites are much lower, in particular for LREE, than those for mantle xenoliths from Vitim (Ionov 2004) and experimental data compiled for pMELTS software (Ghiorso et al. 2002; Jenner and O'Neill 2012), which may be attributed to incomplete equilibration between garnet and cpx (Simon et al. 2003). Data for opx are less precise because of abundances 1–3 orders of magnitude lower than for garnet and cpx. In general, their REE patterns resemble those in coexisting cpx both in coarse and deformed peridotites (Online Resource 4).

Trace element compositions of WR peridotites are listed in Online Resource 1 and illustrated in Online Resource 4. Their patterns for highly to moderately incompatible elements (MREE to Th) are similar to those of host kimberlites (Kamenetsky et al. 2012) and appear to be mainly controlled by contamination with host magmas, consistent with evidence for kimberlite-related interstitial material. By contrast, the HREE patterns (a decrease from Lu to Tm) are opposite to those of the kimberlites and may be similar to those in the mantle source for peridotites. Similar observations were reported from other cratonic garnet peridotite suites (Wittig et al. 2008).

To estimate REE abundances in peridotites before contamination by the host magma, we calculate them from modal compositions and mineral LA-ICPMS data (Online Resources 1 and 4). The contamination-free compositions of coarse peridotites show continuous HREE-depletions from Lu to Ho or spoon-shaped HREE-MREE (Online Resource 4), except for U501, which has a flat pattern. Deformed peridotites have sinusoidal, flat and humped patterns, except for U4, which shows depletion from Lu to Tb and enrichment from Tb to La. These estimates may be a better approximation to "true" HREE-MREE abundances in peridotites than measured ones because these elements in mantle peridotites mainly reside in major minerals

(rather than in accessories and interstitially) (Bedini and Bodinier 1999; Eggins et al. 1998; Sharygin et al. 2007).

Pristine melting residues among garnet peridotites and their formation conditions

To identify "residual" garnet peridotites, whose modal and major element compositions have largely remained intact after partial melting, we compare them with experimental results on melting of fertile mantle (Herzberg 2004; Herzberg and O'Hara 2002; Walter 1998, 2003) and with low-opx spinel harzburgite xenoliths from Udachnaya, which were previously interpreted as melting residues (Doucet et al. 2012). Seven out of 13 coarse garnet peridotites in this study (Uv02/03, Uv419/09, Uv604/09, U29, U260, U506 and U1147) overlap the trend defined on the diagram of bulk-rock Al_2O_3 versus FeO (Fig. 4a) by the spinel harzburgites and also are close to them on plots versus SiO_2, TiO_2 and NiO (Fig. 4c, d, f). Their modal averages (76 % olivine, 16 % opx, <3 % cpx, 4 % gar) and $Mg\#_{Ol}$ (0.923) are similar to those for the spinel harzburgites as well (Figs. 5c and 9); these values may represent the compositional range for the initial residual protolith during craton formation.

Comparisons with experimental data indicate that degrees and depth of partial melting for these rocks appear to be similar to those for the Udachnaya spinel harzburgites. All these rocks overlap lines of equal melt extraction (~45 % anhydrous batch melting or ~38 % fractional melting) as a function of pressure (Fig. 4a). It is also possible that some garnet peridotites were formed by somewhat lower melting degrees, down to 30 %, if their iron contents have not been affected by metasomatism (Fig. 9). To sum up, the protolith of garnet peridotites was formed by 30–38 % of fractional polybaric melt extraction, which began at 7–4 GPa and ended at ≤1–3 GPa (Doucet et al. 2012).

Depth range of melting may have important consequences on Cr contents and Cr/Al ratios in the residues because Cr is much more compatible in spinel than in garnet (Canil 2004). Extended melting in the spinel stability field produces Cr-rich residues, whereas melting in the garnet stability field yields Cr-poor residues. The contents of Cr_2O_3 in the majority of cratonic peridotites, reported in the literature, are much higher (>0.45 %) than in reliable data on fertile to refractory massif peridotites and off-craton peridotite xenoliths (Fig. 4e). This has been interpreted as a result of high degrees of melt extraction in shallow, spinel-facies mantle (Canil 2004; Lee et al. 2011), even though well-documented harzburgite series formed by melt extraction in shallow mantle do not normally show Cr_2O_3 >0.45 % (Ionov 2010; Takazawa et al. 2000). By contrast, Cr_2O_3 in the majority of Udachnaya garnet peridotites are similar to those in off-craton peridotites and are positively correlated with Al_2O_3 (Fig. 4e). Four Udachnaya garnet peridotites have Cr_2O_3 ≥0.5 %, but three of them are deformed, and their high Cr could be due to mechanical sorting of garnet (or its crystallization) in shear zones, complementary to low Cr_2O_3 (≤0.3 %) in four other deformed xenoliths.

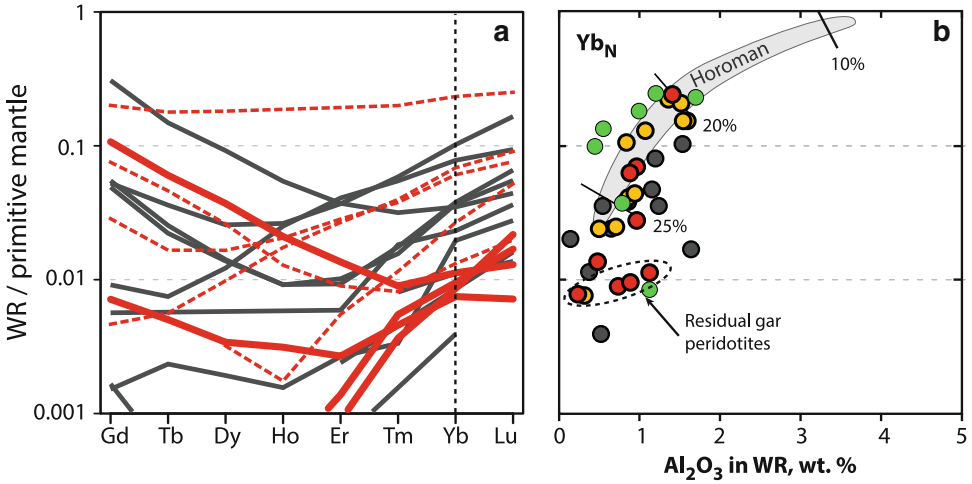

Fig. 10 **a** Primitive mantle-normalized (McDonough and Sun 1995) whole-rock MREE-HREE patterns for coarse garnet peridotites in this study (*red*) and residual spinel peridotites from Udachnaya (Doucet et al. 2012); continuous thick *red lines* show xenoliths from this study with HREE patterns of melting residues unaffected by post-melting processes. **b** Whole-rock abundances of Yb normalized to primitive mantle (Yb_N) for Udachnaya garnet (this study) and spinel peridotite xenoliths (Doucet et al. 2012) in comparison with those in whole-rock Horoman peridotites (Takazawa et al. 2000) and results of trace element modelling for non-modal fractional melting of primitive mantle (McDonough and Sun 1995) modified after Johnson (1998) and Simon et al. (2007) taking into account modal variation of cpx and garnet during decompression melting at 5–1 GPa

The Cr_2O_3 variation range in all but three deformed Udachnaya garnet peridotites is not likely to be due to "nugget effect", advocated by Canil (2004) because our samples are large (Table 1) and because of the excellent positive correlation between Cr_2O_3 or Cr# in garnet with Cr# in bulk-rocks ($r^2 = 0.8$–0.9; Fig. 5e, g), which shows that $Cr\#_{gar}$ and $Cr\#_{WR}$ are equilibrated. The low Cr_2O_3 in both garnet and spinel peridotites suggest that partial melting mainly took place in the garnet stability field, leading to Cr-depletion in the residues, whereas residual garnet was absent or rapidly exhausted for the rocks with $\geq$0.4 % Cr_2O_3. By contrast to our Udachnaya suite, the majority of cratonic peridotite xenoliths reported in the literature shows much higher $Cr\#_{WR}$ than $Cr\#_{gar}$ (Fig. 5e). For some rocks, this might be due to local chemical disequilibrium, for example, for recently formed garnets. We argue, however, that in many cases, this could be related to analytical problems, in particular when Cr, unlike in this study, is not determined by XRF in fused discs, but analysed separately as a "trace element".

Heavy REE are sensitive to the presence of garnet during mantle melting due to high garnet/melt partition coefficients and can be used to constrain depth and degrees of melting (Canil 2004; Simon et al. 2007; Wittig et al. 2008). The broad HREE range in calculated whole-rocks (Fig. 10a) may be mainly controlled by modal garnet in the residues. Figure 10b shows Yb abundances in melting residues of primitive mantle (McDonough and Sun 1995) estimated after Johnson (1998) and Simon et al. (2007) from 5 to 1 GPa (Fig. 10b), which takes into account modal garnet variations in experimental residues (Fig. 6b, c). This modelling shows that melting in the garnet stability field may produce HREE-depleted melting residues. However, our modelling does not consider the change of melting parameters (i.e. P, melting reaction, trace element partition coefficients, etc.) during decompression melting, by contrast with thermodynamic modelling (e.g. pMELTS, calibrated for melting from 1 to 3 GPa [Ghiorso et al. 2002)]. This can produce uncertainties in trace element behaviour during melting. Contamination-free whole-rock HREE of residual coarse garnet peridotites are too low for residues of 35–45 % of melting in the garnet stability field starting at 3 and 5 GPa and may require at least 20–25 % melting of spinel facies. This is generally in agreement with the estimates of melting degrees and pressures from major oxide data ($\sim$30–40 % between 7 and 4 and $\leq$1–3 GPa) and Cr_2O_3 contents.

One coarse, and nearly all deformed garnet peridotites, has nearly flat or Gd–Tm-enriched (Lu < Gd) patterns, which cannot be produced by melt extraction, and are therefore the result of metasomatism.

The origin of garnet and cpx and their modal variations

Garnet and cpx in cratonic peridotites may have different origins: (1) residual phases after melt extraction, (2) exsolution from high-T, Ca–Al-rich opx on cooling and (3) post-melting enrichments. Experiments give useful but limited hints on garnet and cpx abundances in melting residues. The majority of experimental studies on fertile mantle melting address major element compositions of the residues (Herzberg 2004; Herzberg and O'Hara 2002; Walter 1998), but give limited results on their modal abundances, for example, Walter (1998) provides modal compositions of melting residues only for batch melting at 3 and 7 GPa. Here, we use the well-defined correlation between whole-rock Al_2O_3 and modal garnet in cratonic peridotites (Fig. 5h) expressed as: Modal garnet (%) = Al_2O_3 (wt% in WR) $\times$ 5−0.15 ($\pm$1.5 %) to estimate modal garnet in melting residues from data sets of Herzberg (2004) for polybaric fractional melting (starting at 2, 3, 5 and 7 GPa; Fig. 6b) and isobaric batch melting (at 2, 4 and 6 GPa; Fig. 6c). The estimates show that melting residues (re-equilibrated at lower T's in the lithospheric mantle after the melting) may contain up to 5 % of garnet after 35–40 % of polybaric fractional melting starting at high P (5 and 7 GPa), but that garnet is exhausted after 30 % of melt extraction starting at lower P (Fig. 6b). Garnet is more stable during isobaric batch melting [Fig. 6c and Walter (1998)]. About 2/3 of Udachnaya garnet peridotites (i.e. 2/3 coarse and 1/2 deformed) have $\leq$5 % garnet (Fig. 5h). The modal garnet maximum for the whole suite is 4.8 % (Fig. 6a). Hence, garnet in many coarse and transitional peridotites from Udachnaya may be a residual phase after partial melting, like olivine and opx, which is also consistent with depletions from Lu to Gd in such garnets (Fig. 8a, b). By comparison, garnet in xenoliths with >5 % garnet, as well as LREE-MREE enrichments in all garnets, must be a result of post-melting processes (Shimizu 1999; Shimizu et al. 1997; Simon et al. 2003).

Melting experiments and studies of natural residual peridotites show that melting residues may contain small amounts of cpx (up to 2.5 %), for example, due to exsolution from residual opx (Canil and Wei 1992; Saltzer et al. 2001; Takazawa et al. 2000; Walter 1998; Wood and Banno 1973). The majority of Udachnaya garnet peridotites have modal cpx >2.5 %. Moreover, poor correlation of Mg# in cpx and in coexisting olivine (Fig. 5a), together with REE disequilibrium between cpx and garnet (Fig. 8d), indicate that cpx may not be chemically equilibrated with olivine in some rocks. This cpx may be post-melting, late-stage in origin (Canil and Wei 1992; Saltzer et al. 2001; Simon et al. 2003).

The variation ranges of FeO (6.4–8.4 %), TiO_2 (0.02–0.15 %) and $Mg\#_{WR}$ (0.90–0.92) in the Udachnaya garnet peridotites can be viewed as trends of Fe–Ti enrichments of initial melting residues represented by spinel harzburgites (Fig. 4), similar to those described in many cratonic xenolith suites (Ionov et al. 2005b; Kopylova and Russell 2000; Lee and Rudnick 1999; Rudnick et al. 1993; Wittig et al. 2008). Garnet and cpx abundances of Udachnaya peridotites correlate positively with FeO (Fig. 9) and negatively with $Mg\#_{WR}$. These trends, for cratonic peridotites from Udachnaya and elsewhere, are interpreted here as a result of interaction between residual protoliths of garnet peridotites, produced in a range of pressures, with liquids, which precipitated cpx and garnet either during or after craton formation. These processes generally affect deformed peridotites more than coarse peridotites.

Mantle metasomatism in time and space

Peridotite xenoliths from Udachnaya, which equilibrated at <5.5 GPa (i.e. coarse garnet and spinel peridotites), tend to have higher $Mg\#_{Ol}$, $Mg\#_{WR}$ and lower HREE than predominantly deformed peridotites equilibrated at >5.5 GPa (Figs. 4b and 5a and Online Resource 4). The upper part of the lithospheric profile has better preserved the chemical compositions of its residual protoliths than the lower part as earlier inferred for the Siberian (Boyd et al. 1997; Ionov et al. 2010), Kaapvaal (Boyd and Mertzman 1987; Simon et al. 2007) and Slave cratons (Kopylova and Russell 2000; Kopylova et al. 1999). However, we find no clear correlation of melt depletion and metasomatism indices with equilibration temperature or depth for Udachnaya garnet peridotites. This contrasts with the increase in "fertility" (lower $Mg\#_{WR}$, higher cpx) with depth documented in the Slave craton (Kopylova and Russell 2000). Despite the absence of clear relationships between the *P–T* values, deformation degrees and the magnitude of metasomatism, the majority of sheared garnet peridotites have the lowest $Mg\#_{WR}$, highest FeO, and greatest trace element enrichments in whole-rock, cpx and garnet. This strongly suggests that the deformation may be contemporary to metasomatism.

Peridotites in this study have complex contamination-free whole-rock trace element compositions, which cannot be produced by a single process. HREE in residual garnet peridotites can be explained by high degrees of melt extraction, whereas LREE-MREE may reflect post-melting enrichments (Fig. 10). We have shown that the cpx compositions in the Udachnaya garnet peridotites are most likely linked to metasomatism. To constrain the nature of metasomatic agents that produced incompatible element enrichment of the cpx (and possibly of some garnets), we calculated the REE contents of hypothetical melts in equilibrium with cpx in the xenoliths (Fig. 11). The calculated REE ranges in the melts are similar to those in the Udachnaya kimberlites (Kamenetsky et al. 2012).

Some previous studies (Simon et al. 2003; Stachel and Harris 1997) linked kimberlite circulation in the lithospheric mantle to crystallization of phlogopite and cpx in peridotite xenoliths following the reaction: gar + opx + fluid → phlogopite + diopside (Boyd et al. 1997; Grégoire et al. 2002; van Achterbergh et al. 2001). The majority of garnet and spinel peridotites from Udachnaya in this and related studies (Doucet et al. 2012; Ionov et al. 2010) are mica-free. Phlogopite, when present, only occurs as a late-stage phase related to kimberlite veins (Online

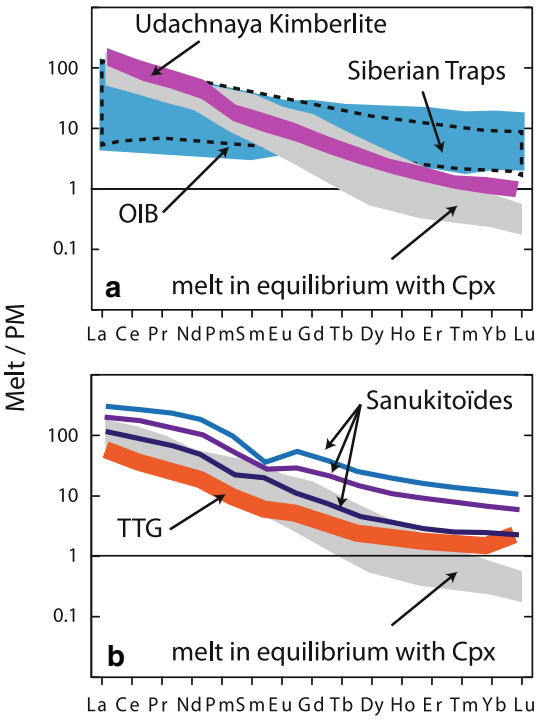

Fig. 11 Primitive mantle-normalized (McDonough and Sun 1995) REE field for hypothetical melts in equilibrium with cpx (*grey* field) calculated using mineral/melt partition coefficients compiled for pMELTS software (Ghiorso et al. 2002; Smith and Asimow 2005). Also shown are Udachnaya kimberlite compositions (*pink* field; Kamenetsky et al. 2012) (**a**), Siberian trap basalts (*blue* field; (Hawkesworth and Gallaher 1993; Hawkesworth et al. 1995; Kamo et al. 2003; Lightfoot et al. 1990; Reichow et al. 2005) (**a**), Hawaiian ocean island basalts (fine *dashed line*; (Clague and Moore 2002; Feigenson et al. 2003; Fekiacova et al. 2007; Huang and Frey 2003; Kimura et al. 2006; Lipman et al. 2006; Morgan et al. 2007; Pearce et al. 1999; Ren et al. 2009; Sims et al. 1999; Van Der Zander et al. 2010; Wanless et al. 2006; Xu et al. 2005) (**a**), South African Tonalite-Trondhjemite-Granodiorite (TTG, orange field; Martin and Moyen 2002) (**b**) and South African sanukitoïdes (MME (microgranular mafic enclaves), clear *blue* field; enderbite, *dark purple* field; mafic dykes, *dark blue* filed; Laurent et al. 2011) (**b**). Udachnaya kimberlite melts appear to be the best potential metasomatic agents to account for the cpx compositions

Resource 3). The common chemical homogeneity of minerals and local disequilibrium between cpx and garnet indicate that the kimberlite veins must have been emplaced shortly before kimberlite eruption that brought up the xenoliths to the surface.

Conclusions

1. Coarse and deformed garnet peridotites in this study span a *P–T* range from 2.5 to 6.6 GPa and 720–1,320 °C. They range from near-pristine melting residues to Fe–Ti-enriched rocks. About ½ of coarse peridotites are similar in modal, major and trace element compositions to low-opx Udachnaya spinel harzburgites previously interpreted as melting residues. The protoliths of the garnet peridotites may have been formed by 30–38 % of anhydrous polybaric partial melting between 7 and 4 GPa and ≤1–3 GPa, that is, at similar or slightly lower melting degrees than the spinel harzburgites.
2. Garnets in many coarse and transitional Udachnaya xenoliths with ≤5 % of modal garnet, as well as in other cratonic peridotites, may be residual phases that survived partial melting.
3. The majority of Udachnaya garnet peridotites experienced modal metasomatism, which precipitated cpx and HREE-MREE-rich garnets and produced enrichments in Fe, Ti, Al and Ca. The metasomatism can be linked to a range of silicate- and carbonate-rich liquids. The latest event took place shortly before the kimberlite eruption and was related to localized deformation.

Acknowledgments We thank the ALROSA joint stock company and the open-pit mine staff for access to the site and assistance with sample collection, N. P. Pokhilenko for support in Novosibirsk, P. Nimis for *P–T* calculation spreadsheet, P. Bowden for improving the quality of early versions of the manuscript and C. Alboussière, C. Perrache and J. L. Devidal for analytical and technical assistance. Comments of two anonymous reviewers helped to improve the paper. The research was supported by funding from INSU-CNRS, France (PICS project N5812 and PNP projects in 2010–2012) and grants No 11-05-91060-PICS and No 13-05-00439 of the Russian Foundation for Basic Research.

References

Agashev AM, Ionov DA, Pokhilenko NP, Golovin AV, Cherepanova Yu, Sharygin IS (2013) Metasomatism in lithospheric mantle roots: constraints from whole-rock and mineral chemical composition of deformed peridotite xenoliths from kimberlite pipe Udachnaya. Lithos 160–161:201–215. doi:10.1016/j.lithos.2012.11.014

Ashchepkov IV, Pokhilenko NP, Vladykin NV, Logvinova AM, Afanasiev VP, Pokhilenko LN, Kuligin SS, Malygina EV, Alymova NA, Kostrovitsky SI, Rotman AY, Mityukhin SI, Karpenko MA, Stegnitsky YB, Khmelnikova OS (2010) Structure and evolution of the lithospheric mantle beneath Siberian craton, thermobarometric study. Tectonophysics 485(1–4):17–41

Bedini RM, Bodinier J-L (1999) Distribution of incompatible trace elements between the constituents of spinel peridotite xenoliths: ICP-MS data from the East African rift. Geochim Cosmochim Acta 63(22):3883–3900

Bernstein S, Kelemen PB, Brooks CK (1998) Depleted spinel harzburgite xenoliths in Tertiary dykes from East Greenland: restites from high degree melting. Earth Planet Sci Lett 154(1–4):219–233

Bernstein S, Kelemen PB, Hanghoj K (2007) Consistent olivine Mg# in cratonic mantle reflects Archean mantle melting to the exhaustion of orthopyroxene. Geology 35(5):459–462

Boyd FR (1989) Compositional distinction between oceanic and cratonic lithosphere. Earth Planet Sci Lett 96:15–26

Boyd FR, Mertzman SA (1987) Composition and structure of the Kaapvaal lithosphere, Southern Africa. In: Mysen BO (ed) Magmatic processes: physicochemical principles, vol 1. Geochemical Society Special Publications 1, pp 3–12

Boyd FR, Pokhilenko NP, Pearson DG, Mertzman SA, Sobolev NV, Finger LW (1997) Composition of the Siberian cratonic mantle: evidence from Udachnaya peridotite xenoliths. Contrib Mineral Petrol 128:228–246

Boyd FR, Pearson DG, Hoal KO, Hoal BG, Nixon PH, Kingston MJ, Mertzman SA (2004) Garnet lherzolites from Louwrensia, Namibia: bulk composition and P/T relations. Lithos 77(1–4):573–592

Brey GP, Köhler T (1990) Geothermobarometry in four-phase lherzolites II. New thermobarometers, and practical assessment of existing thermobarometers. J Petrol 31:1353–1378

Canil D (2004) Mildly incompatible elements in peridotites and the origins of mantle lithosphere. Lithos 77(1–4):375–393

Canil D, Wei KJ (1992) Constraints on the origin of mantle-derived low Ca garnets. Contrib Mineral Petrol 109(4):421–430

Carlson RW, Pearson DG, James DE (2005) Physical, chemical, and chronological characteristics of continental mantle. Rev Geophys 43:RG1001. doi:10.1029/2004RG000156

Clague DA, Moore JG (2002) The proximal part of the giant submarine Wailau landslide, Molokai, Hawaii. J Volcanol Geotherm Res 113(1–2):259–287. doi:10.1016/s0377-0273(01)00261-x

Creighton S (2009) A semi-empirical manganese-in-garnet single crystal thermometer. Lithos 112(Suppl 1 (0)):177–182. doi:10.1016/j.lithos.2009.05.011

Delaney JS, Smith JV, Dawson JB, Nixon PH (1979) Manganese thermometer for mantle peridotites. Contrib Mineral Petrol 71(2):157–169. doi:10.1007/BF00375432

Doucet LS, Ionov DA, Golovin AV, Pokhilenko NP (2012) Depth, degrees and tectonic settings of mantle melting during craton formation: inferences from major and trace element compositions of spinel harzburgite xenoliths from the Udachnaya kimberlite, central Siberia. Earth Planet Sci Lett 359–360:206–218. doi:10.1016/j.epsl.2012.10.001

Eggins SM, Rudnick RL, McDonough WF (1998) The composition of peridotites and their minerals: a laser ablation ICP-MS study. Earth Planet Sci Lett 154:53–71

Feigenson MD, Bolge LL, Carr MJ, Herzberg CT (2003) REE inverse modeling of HSDP2 basalts: evidence for multiple sources in the Hawaiian plume. Geochem Geophys Geosyst 4(2):8706. doi:10.1029/2001gc000271

Fekiacova Z, Abouchami W, Galer SJG, Garcia MO, Hofmann AW (2007) Origin and temporal evolution of Koólau Volcano, Hawaii: inferences from isotope data on the Koólau Scientific Drilling Project (KSDP), the Honolulu Volcanics and ODP Site

843. Earth Planet Sci Lett 261(1–2):65–83. doi:10.1016/j.epsl.2007.06.005
Gagnon JE, Fryer BJ, Samson IM, Williams-Jones AE (2008) Quantitative analysis of silicate certified reference materials by LA-ICPMS with and without an internal standard. J Analyt Atom Spectrom 23:1529–1537. doi:10.1039/b801807n
Ghiorso MS, Hirschmann MM, Reiners PW, Kress VC (2002) The pMELTS: a revision of MELTS for improved calculation of phase relations and major element partitioning related to partial melting of the mantle to 3 GPa. Geochem Geophys Geosyst 3(5):1030. doi:10.1029/2001gc000217
Goncharov AG, Ionov DA, Doucet LS, Pokhilenko LN (2012) Thermal state, oxygen fugacity and C-O-H fluid speciation in cratonic lithospheric mantle: new data on peridotite xenoliths from the Udachnaya kimberlite, Siberia. Earth Planet Sci Lett 357–358:99–110. doi:10.1016/j.epsl.2012.09.016
Grégoire M, Bell DR, Le Roex AP (2002) Trace element geochemistry of phlogopite-rich mafic mantle xenoliths: their classification and their relationship to phlogopite-bearing peridotites and kimberlites revisited. Contrib Mineral Petrol 142(5):603–625
Griffin WL, Ryan CG, Kaminsky FV, O'Reilly SY, Natapov LM, Win TT, Kinny PD, Ilupin IP (1999) The Siberian lithosphere traverse: mantle terranes and the assembly of the Siberian Craton. Tectonophysics 310(1–4):1–35
Grütter HS, Gurney JJ, Menzies AH, Winter F (2004) An updated classification scheme for mantle-derived garnet, for use by diamond explorers. Lithos 77:841–857
Hawkesworth CJ, Gallaher K (1993) Mantle hotspots, plumes and regional tectonics as causes of intraplate magmatism. Terra Nova 5:552–559
Hawkesworth CJ, Lightfoot PC, Fedorenko VA, Blake S, Naldrett AJ, Doherty W, Gorbachev NS (1995) Magma differentiation and mineralisation in the Siberian continental flood basalts. Lithos 34(1–3):61–88. doi:10.1016/0024-4937(95)90011-x
Herzberg C (2004) Geodynamic information in peridotite petrology. J Petrol 45(12):2507–2530
Herzberg C, O'Hara MJ (2002) Plume-associated ultramafic magmas of Phanerozoic age. J Petrol 43(10):1857–1883
Huang S, Frey FA (2003) Trace element abundances of Mauna Kea basalt from phase 2 of the Hawaii Scientific Drilling Project: petrogenetic implications of correlations with major element content and isotopic ratios. Geochem Geophys Geosyst 4(6):8711. doi:10.1029/2002gc000322
Ionov DA (2004) Chemical variations in peridotite xenoliths from Vitim, Siberia: inferences for REE and Hf behaviour in the garnet facies upper mantle. J Petrol 45(2):343–367. doi:10.1093/petrology/egg090
Ionov DA (2010) Petrology of mantle wedge lithosphere: new data on supra-subduction zone peridotite xenoliths from the andesitic Avacha volcano, Kamchatka. J Petrol 51(1–2):327–361. doi:10.1093/petrology/egp090
Ionov DA, Hofmann AW (2007) Depth of formation of sub-continental off-craton peridotites. Earth Planet Sci Lett 261(3–4):620–634. doi:10.1016/j.epsl.2007.07.036
Ionov DA, Savoyant L, Dupuy C (1992) Application of the ICP-MS technique to trace element analysis of peridotites and their minerals. Geostand Newsl 16(2):311–315
Ionov DA, Ashchepkov I, Jagoutz E (2005a) The provenance of fertile off-craton lithospheric mantle: Sr-Nd isotope and chemical composition of garnet and spinel peridotite xenoliths from Vitim, Siberia. Chem Geol 217(1–2):41–75. doi:10.1016/j.chemgeo.2004.12.001
Ionov DA, Chanefo I, Bodinier J-L (2005b) Origin of Fe-rich lherzolites and wehrlites from Tok, SE Siberia by reactive melt percolation in refractory mantle peridotites. Contrib Mineral Petrol 150(3):335–353
Ionov DA, Doucet LS, Ashchepkov IV (2010) Composition of the lithospheric mantle in the Siberian craton: new constraints from fresh peridotites in the Udachnaya-East kimberlite. J Petrol 51(11):2177–2210. doi:10.1093/petrology/egq053
Irvine GJ, Pearson DG, Kjarsgaard BA, Carlson RW, Kopylova MG, Dreibus G (2003) A Re-Os isotope and PGE study of kimberlite-derived peridotite xenoliths from Somerset Island and a comparison to the Slave and Kaapvaal cratons. Lithos 71(2–4):461–488
Jenner FE, O'Neill HSC (2012) Analysis of 60 elements in 616 ocean floor basaltic glasses. Geochem Geophys Geosyst 13:Q02005. doi:10.1029/2011gc004009
Johnson KTM (1998) Experimental determination of partition coefficients for rare earth and high-field-strength elements between clinopyroxene, garnet, and basaltic melt at high pressures. Contrib Mineral Petrol 133:60–68
Kamenetsky VS, Kamenetsky MB, Sobolev AV, Golovin AV, Demouchy S, Faure K, Sharygin VV, Kuzmin DV (2008) Olivine in the Udachnaya-East kimberlite (Yakutia, Russia): types, compositions and origins. J Petrol 49(4):823–839. doi:10.1093/petrology/egm033
Kamenetsky VS, Kamenetsky MB, Sobolev AV, Golovin AV, Sharygin VV, Pokhilenko NP, Sobolev NV (2009a) Can pyroxenes be liquidus minerals in the kimberlite magma? Lithos 112(Supplement 1):213–222. doi:10.1016/j.lithos.2009.03.040
Kamenetsky VS, Maas R, Kamenetsky MB, Paton C, Phillips D, Golovin AV, Gornova MA (2009b) Chlorine from the mantle: magmatic halides in the Udachnaya-East kimberlite, Siberia. Earth Planet Sci Lett 285(1–2):96–104. doi:10.1016/j.epsl.2009.06.001
Kamenetsky VS, Kamenetsky MB, Golovin AV, Sharygin VV, Maas R (2012) Ultrafresh salty kimberlite of the Udachnaya–East pipe (Yakutia, Russia): a petrological oddity or fortuitous discovery? Lithos 152:173–186. doi:10.1016/j.lithos.2012.1004.1032
Kamo SL, Czamanske GK, Amelin Y, Fedorenko VA, Davis DW, Trofimov VR (2003) Rapid eruption of Siberian flood-volcanic rocks and evidence for coincidence with the Permian–Triassic boundary and mass extinction at 251 Ma. Earth Planet Sci Lett 214(1–2):75–91. doi:10.1016/s0012-821x(03)00347-9
Kelemen PB, Hart SR, Bernstein S (1998) Silica enrichment in the continental upper mantle via melt/rock reaction. Earth Planet Sci Lett 164(1–2):387–406
Kimura J-I, Sisson TW, Nakano N, Coombs ML, Lipman PW (2006) Isotope geochemistry of early Kilauea magmas from the submarine Hilina bench: the nature of the Hilina mantle component. J Volcanol Geotherm Res 151(1–3):51–72. doi:10.1016/j.jvolgeores.2005.07.024
Kinny PD, Griffin BJ, Heaman LM, Brakhfogel FF, Spetsius ZV (1997) SHRIMP U-Pb ages of perovskite from Yakutian kimberlites. Geol Geofiz 38(1):91–99 (in Russian)
Kopylova MG, Caro G (2004) Mantle xenoliths from the southeastern Slave craton: evidence for chemical zonation in a thick, cold Lithosphere. J Petrol 45(5):1045–1067
Kopylova MG, Russell JK (2000) Chemical stratification of cratonic lithosphere: constraints from the Northern Slave craton, Canada. Earth Planet Sci Lett 181(1–2):71–87
Kopylova MG, Russell JK, Cookenboo H (1999) Petrology of peridotite and pyroxenite xenoliths from the Jerico kimberlite: implications for the thermal state of the mantle beneath the Slave craton, Northern Canada. J Petrol 40(1):79–104
Laurent O, Martin H, Doucelance R, Moyen JF, Paquette JL (2011) Geochemistry and petrogenesis of high-K "sanukitoids" from the Bulai pluton, Central Limpopo Belt, South Africa: implications for geodynamic changes at the Archaean-Proterozoic boundary. Lithos 123(1–4):73–91

Lee C-T, Rudnick RL (1999) Compositionally stratified cratonic lithosphere: petrology and geochemistry of peridotite xenoliths the Labait volcano, Tanzania. In: Gurney JJ, Gurney JL, Pascoe MD, Richardson SH (eds) Proceedings of 7th International Kimberlite Conference, vol I: The Dawson Volume. RedRoof Design, Cape Town, pp 503–521

Lee C-TA, Luffi P, Chin EJ (2011) Building and destroying continental mantle. In: Jeanloz R, Freeman K (eds) Ann Rev Earth and Planet Sci 39:59-90

Lightfoot PC, Naldrett AJ, Gorbachev NS, Doherty W, Fedorenko VA (1990) Geochemistry of the Siberian Trap of the Noril'sk area, USSR, with implications for the relative contributions of crust and mantle to flood basalt magmatism. Contrib Mineral Petrol 104(6):631–644. doi:10.1007/bf01167284

Lipman PW, Sisson TW, Coombs ML, Calvert A, Kimura J-I (2006) Piggyback tectonics: long-term growth of Kilauea on the south flank of Mauna Loa. J Volcanol Geotherm Res 151(1–3):73–108. doi:10.1016/j.jvolgeores.2005.07.032

Martin H, Moyen JF (2002) Secular changes in tonalite-trondhjemite-granodiorite composition as markers of the progressive cooling of Earth. Geology 30(4):319–322

McDonough WF, Sun S–S (1995) The composition of the Earth. Chem Geol 120:223–253

Morgan JK, Clague DA, Borchers DC, Davis AS, Milliken KL (2007) Mauna Loa's submarine western flank: landsliding, deep volcanic spreading, and hydrothermal alteration. Geochem Geophys Geosyst 8(5):Q05002. doi:10.1029/2006gc001420

Mori T, Green DH (1978) Laboratory duplication of phase equilibria observed in natural garnet lherzolites. J Geol 86:83–97

Nickel KG, Green DH (1985) Empirical geothermobarometry for garnet peridotites and implications for the nature of the lithosphere, kimberlites and diamonds. Earth Planet Sci Lett 73:158–170

Nimis P, Grütter H (2010) Internally consistent geothermometers for garnet peridotites and pyroxenites. Contrib Mineral Petrol 159(3):411–427

Nimis P, Taylor WR (2000) Single clinopyroxene thermobarometry for garnet peridotites. Part I. Calibration and testing of a Cr-in-Cpx barometer and an enstatite-in-Cpx thermometer. Contrib Mineral Petrol 139(5):541–554. doi:10.1007/s004100000156

Pearce JA, Kempton PD, Nowell GM, Noble SR (1999) Hf-Nd element and isotope perspective on the nature and provenance of mantle and subduction components in Western Pacific arc-basin systems. J Petrol 40(11):1579–1611. doi:10.1093/petroj/40.11.1579

Pearson DG, Wittig N (2008) Formation of Archaean continental lithosphere and its diamonds: the root of the problem. J Geol Soc London 165(5):895–914

Pearson DG, Carlson RW, Shirey SB, Boyd FR, Nixon PH (1995) Stabilisation of Archaen lithospheric mantle: a Re-Os isotope study of peridotite xenoliths from the Kaapvaal craton. Earth Planet Sci Lett 134:341–357

Pearson DG, Canil D, Shirey SB (2003) Mantle samples included in volcanic rocks: xenoliths and diamonds. In: Carlson RW (ed) Treatise on geochemistry, the mantle and core, vol 2. Elsevier, Amsterdam, pp 171–276

Pearson DG, Irvine GJ, Ionov DA, Boyd FR, Dreibus GE (2004) Re-Os isotope systematics and platinum group element fractionation during mantle melt extraction: a study of massif and xenolith peridotite suites. Chem Geol 208(1–4, Highly Siderophile Element Behavior in High Temperature Processes):29–59

Pollack HN, Chapman DS (1977) On the regional variation of heat flow, geotherms and lithospheric thickness. Tectonophysics 38:279–296

Reichow MK, Saunders AD, White RV, Al'Mukhamedov AI, Medvedev AY (2005) Geochemistry and petrogenesis of basalts from the West Siberian Basin: an extension of the Permo–Triassic Siberian Traps, Russia. Lithos 79(3–4):425–452. doi:10.1016/j.lithos.2004.09.011

Ren Z-Y, Hanyu T, Miyazaki T, Chang Q, Kawabata H, Takahashi T, Hirahara Y, Nichols ARL, Tatsumi Y (2009) Geochemical differences of the Hawaiian shield lavas: implications for melting process in the heterogeneous Hawaiian plume. J Petrol 50(8):1553–1573. doi:10.1093/petrology/egp041

Rosen OM, Condie KC, Natapov LM, Nozhkin AD (1994) Archean and Early Proterozoic evolution of the Siberian craton: a preliminary assessment. In: Condie KC (ed) Archean crustal evolution. Elsevier, Amsterdam, pp 411–459

Rudnick RL, Nyblade AA (1999) The thickness and heat production of Archean lithosphere: constraints from xenolith thermobarometry and surface heat flow. In: Fei Y, Bertka CM, Mysen BO (eds) Mantle petrology: field observations and high-pressure experimentation. Spec Publ Geochem Soc No 6, vol. Geochemical Society, Houston, pp 3–12

Rudnick RL, McDonough WF, Chappell BC (1993) Carbonatite metasomatism in the northern Tanzanian mantle. Earth Planet Sci Lett 114:463–475

Ryan CG, Griffin WL, Pearson NJ (1996) Garnet geotherms: pressure-temperature data from Cr-pyrope garnet xenocrysts in volcanic rocks. J Geophys Res 101(B3):5611–5625

Saltzer RL, Chatterjee N, Grove TL (2001) The spatial distribution of garnets and pyroxenes in mantle peridotites: pressure–temperature history of peridotites from the Kaapvaal Craton. J Petrol 42(12):2215–2229. doi:10.1093/petrology/42.12.2215

Sand KK, Waight TE, Pearson DG, Nielsen TFD, Makovicky E, Hutchison MT (2009) The lithospheric mantle below southern West Greenland: a geothermobarometric approach to diamond potential and mantle stratigraphy. Lithos 112(Supplement 2):1155–1166

Sharygin VV, Golovin AV, Pokhilenko NP, Kamenetsky VS (2007) Djerfisherite in the Udachnaya-East pipe kimberlites (Sakha-Yakutia, Russia): paragenesis, composition and origin. Eur J Mineral 19(1):51–63. doi:10.1127/0935-1221/2007/0019-0051

Shimizu N (1999) Young geochemical features in cratonic peridotites from Southern Africa and Siberia. In: Fei Y, Bertka CM, Mysen BO (eds) Mantle petrology: field observations and high-pressure experimentation Spec Publ Geochem Soc No 6, vol. Geochemical Society, Houston, pp 47–55

Shimizu N, Pokhilenko NP, Boyd FR, Pearson DG (1997) Geochemical characteristics of mantle xenoiliths from the Udachnaya kimberlite pipe. Russ Geol Geophys 38(1):205–217

Simon NSC, Irvine GJ, Davies GR, Pearson DG, Carlson RW (2003) The origin of garnet and clinopyroxene in "depleted" Kaapvaal peridotites. Lithos 71(2–4):289–322

Simon NSC, Carlson RW, Pearson DG, Davies GR (2007) The origin and evolution of the Kaapvaal cratonic lithospheric mantle. J Petrol 48(3):589–625

Sims KWW, DePaolo DJ, Murrell MT, Baldridge WS, Goldstein S, Clague D, Jull M (1999) Porosity of the melting zone and variations in the solid mantle upwelling rate beneath Hawaii: inferences from 238U–230Th-226Ra and 235U–231 Pa disequilibria. Geochim Cosmochim Acta 63(23–24):4119–4138. doi:10.1016/s0016-7037(99)00313-0

Smith PM, Asimow PD (2005) Adiabat_1ph: a new public front-end to the MELTS, pMELTS, and pHMELTS models. Geochem Geophys Geosyst 6(2):Q02004. doi:10.1029/2004gc000816

Sobolev NV (1974) Deep-seated inclusions in kimberlites and the problem of the composition of the upper mantle. Nauka, Novosibirsk

Spetsius ZV, Serenko VP (1990) Composition of the continental upper mantle and lower crust beneath the Siberian platform. Nauka, Moscow

Stachel T, Harris JW (1997) Syngenetic inclusions in diamond from the Birim field (Ghana)—a deep peridotitic profile with a history of depletion and re-enrichment. Contrib Mineral Petrol 127: 336–352

Takazawa E, Frey FA, Shimizu N, Obata M (2000) Whole rock compositional variations in an upper mantle peridotite (Horoman, Hokkaido, Japan): are they consistent with a partial melting process. Geochim Cosmochim Acta 64(4):695–716

Taylor WR (1998) An experimental test of some geothermometer and geobarometer formulations for upper mantle peridotites with application to the thermobarometry of fertile lherzolite and garnet websterite. Neues Jahrbuch fur Mineralogie-Abhandlungen 172(2–3):381–408

van Achterbergh E, Griffin WL, Stiefenhofer J (2001) Metasomatism in mantle xenoliths from the Letlhakane kimberlites: estimation of element fluxes. Contrib Mineral Petrol 141(4):397–414

Van Der Zander I, Sinton JM, Mahoney JJ (2010) Late shield-stage silicic magmatism at Wai'anae volcano: evidence for hydrous crustal melting in Hawaiian volcanoes. J Petrol 51(3):671–701. doi:10.1093/petrology/egp094

Walter MJ (1998) Melting of garnet peridotite and the origin of komatiite and depleted lithosphere. J Petrol 39(1):29–60

Walter MJ (2003) Melt extraction and compositional variability in mantle lithosphere. In: Carlson RW (ed) Treatise on geochemistry vol 2, the mantle and core. Elsevier, Amsterdam, pp 363–394

Wanless VD, Garcia MO, Trusdell FA, Rhodes JM, Norman MD, Weis D, Fornari DJ, Kurz MD, Guillou H (2006) Submarine radial vents on Mauna Loa Volcano, Hawai'i. Geochem Geophys Geosyst 7(5):Q05001. doi:10.1029/2005gc001086

Wittig N, Pearson DG, Webb M, Ottley CJ, Irvine GJ, Kopylova M, Jensen SM, Nowell GM (2008) Origin of cratonic lithospheric mantle roots: a geochemical study of peridotites from the North Atlantic Craton, West Greenland. Earth Planet Sci Lett 274(1–2): 24–33

Wood BJ, Banno S (1973) Garnet-orthopyroxene and orthopyroxene-clinopyroxene relationships in simple and complex systems. Contrib Mineral Petrol 42:109–124

Xu G, Frey FA, Clague DA, Weis D, Beeson MH (2005) East Molokai and other Kea-trend volcanoes: magmatic processes and sources as they migrate away from the Hawaiian hot spot. Geochem Geophys Geosyst 6(5):Q05008. doi:10.1029/2004gc000830

Zinchuk NN, Spetsius ZV, Zuenko VV, Zuev VM (1993) Kimberlite Pipe Udachnaya. Novosibirsk University, Novosibirsk